

SPIKEGRASP: A BENCHMARK FOR 6-DOF GRASP POSE DETECTION FROM STEREO SPIKE STREAMS

Zhuoheng Gao¹ Jiyao Zhang² Zhiyong Xie¹ Hao Dong² Zhaofei Yu^{1,3}
 Rongmei Chen⁴ Guozhang Chen^{1†} Tiejun Huang¹

¹ National Key Laboratory for Multimedia Information Processing, School of Computer Science, Peking University

² Center on Frontiers of Computing Studies, School of Computer Science, Peking University

³ Institute for Artificial Intelligence, Peking University

⁴ School of Electronics, Peking University

gaozh@stu.pku.edu.cn guozhang.chen@pku.edu.cn

ABSTRACT

Most robotic grasping systems rely on converting sensor data into explicit 3D point clouds, which is a computational step not found in biological intelligence. This paper explores a fundamentally different, neuro-inspired paradigm for 6-DoF grasp detection. We introduce SpikeGrasp, a framework that mimics the biological visuomotor pathway, processing raw, asynchronous events from stereo spike cameras, similarly to retinas, to directly infer grasp poses. Our model fuses these stereo spike streams and uses a recurrent spiking neural network, analogous to high-level visual processing, to iteratively refine grasp hypotheses without ever reconstructing a point cloud. To validate this approach, we built a large-scale synthetic benchmark dataset. Experiments show that SpikeGrasp surpasses traditional point-cloud-based baselines, especially in cluttered and textureless scenes, and demonstrates remarkable data efficiency. By establishing the viability of this end-to-end, neuro-inspired approach, SpikeGrasp paves the way for future systems capable of the fluid and efficient manipulation seen in nature, particularly for dynamic objects.

1 INTRODUCTION

The ability to pick up an arbitrary object is a fundamental measure of intelligence for an autonomous robot. The prevailing approach to this grasp detection problem follows a distinct geometry-first pipeline: capture a scene with sensors, reconstruct a 3D geometric model (typically a point cloud) and then analyze this model for a viable grasp (Fang et al., 2020; Gui et al., 2025). This paradigm is logical from a computer graphics perspective, but is a significant departure from how biological systems operate. The brain does not compute or store explicit point clouds to decide how to grasp a coffee cup (Cao et al., 2025); it leverages a continuous stream of sensory information processed through a highly efficient neural architecture. Furthermore, reliance on point cloud reconstruction can be computationally intensive and brittle (Mahler et al., 2017), sensitive to sensor noise and challenging lighting (Deng et al., 2020), limiting robustness for the eventual goal of interacting with dynamic environments (Fang et al., 2023). These two paths are shown in Fig. 1.

This paper investigates a different path, one inspired by the efficiency and elegance of the brain’s visual-motor system. We leverage bio-inspired spike cameras (Zheng et al., 2023), which act as artificial retinas, generating asynchronous streams of spikes that intrinsically capture temporal dynamics. Instead of converting these rich data into a static geometric representation, we ask: Can we create a system that thinks in spikes, not in point clouds, to determine how to act?

To this end, we introduce SpikeGrasp, a novel framework that embodies this neuro-inspired philosophy. Our architecture is conceptually modeled on the primate visual system. Artificial retinas: Stereo spike cameras provide asynchronous, event-based inputs. Visual pathways: Left and right

[†]Corresponding author.

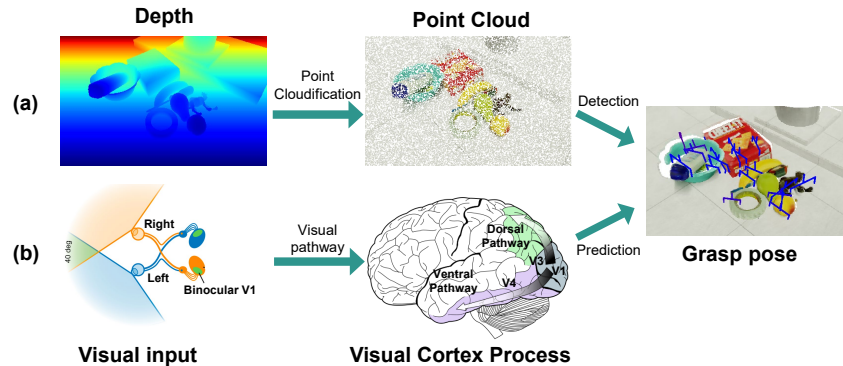


Figure 1: Comparison of two calculation paths. The above (a) is the use of depth input and point cloud reconstruction to detect feasible grasping steps. And the following (b) is the brain obtains information through the visual system, and then processes the information streams through neural architecture to determine how to grasp it.

spike streams are processed and fused, analogous to signals traveling through the brain’s hemispheres. Integrative cortex: Recurrent spiking neural networks act as a high-level integrative area, processing the fused information, and iteratively refining a hidden state that represents the scene’s grasp affordances. Motor system: A final readout network decodes this neural state into a 6-DoF grasp pose, akin to a motor command. Crucially, this entire system learns to map spikes to actions end-to-end, bypassing intermediate geometric representations. Although this paper establishes our method on static scenes, it serves as a critical first step, demonstrating its feasibility.

The main contributions of this paper are as follows:

- We propose a novel biologically inspired SpikeGrasp architecture that refines asynchronous spike data through iterative updates. Experimental results demonstrate that our method surpasses previous methods in detection quality in the synthetic dataset.
- We present the first large-scale synthetic spike stream dataset for 6-DoF grasp pose detection to offer an evaluation benchmark for this emerging field.
- We demonstrate the data efficiency of the proposed framework, highlighting the strong generalization even with limited training samples.

2 RELATED WORK

2.1 METHODS USING POINT CLOUD INPUTS

A large body of 6-DoF grasp estimations is based on explicit geometric inputs. Sampling–evaluation pipelines such as GPD (Ten Pas et al., 2017) and PointNetGPD (Liang et al., 2019) generate candidates with dense grasp and rank them with a learned quality model. End-to-end approaches directly process geometric representations to regress feasible 6-DoF grasps, including variational proposal generation in GraspNet (Fang et al., 2020), volumetric or point-based predictors (Breyer et al., 2021; Qin et al., 2020; Ni et al., 2020), and RGB-D fusion schemes that improve depth noise robustness (AVN (Gou et al., 2021)). The graspability per point maps further guide the prediction (GSNet (Wang et al., 2021), AnyGrasp (Fang et al., 2023)), while contextual reasoning enhances scene awareness (VoteGrasp (Hoang et al., 2022)). Joint formulations integrate segmentation with grasp estimation (Liu et al., 2023), heatmap-based parameterization streamlines inference (Chen et al., 2024), and cross-modal refinement leverages RGB to denoise depth (DGCAN (Qin et al., 2023)). Because many of these methods treat scenes as purely geometric sets, Contact-graspnet (Sundermeyer et al., 2021) adds a two-stage pipeline with unknown object instance segmentation (Xie et al., 2021). Recent efforts also emphasize efficiency and scalability, e.g., GraspFast (Gui et al., 2025) and ZeroGrasp (Iwase et al., 2025). Collectively, point-cloud or depth-based pipelines remain the dominant paradigm due to their explicit 3D constraints and mature tooling.

2.2 METHODS WITHOUT EXPLICIT POINT CLOUD

An alternative line of work avoids explicit depth or point clouds by predicting grasps directly from images or implicit 3D representations. Although simple and fast, their low degrees of freedom limit their applicability in cluttered, contact-rich settings. In contrast to the depth-centric methods above, approaches that infer full 6-DoF grasps without explicit geometric inputs, such as by aggregating multi-view cues or adopting neural field-style scene encodings (Jauhri et al., 2023; Shi et al., 2024; Dai et al., 2022b). This gap highlights an opportunity for methods that recover graspable structure from raw image streams or other non-depth signals while retaining the expressivity of 6-DoF grasp reasoning. In addition, a complementary direction uses neuromorphic sensing, such as event/spike cameras, to drive grasp reasoning without explicit depth by reporting asynchronous changes at microsecond latency. Such inputs offer high dynamic range and low motion blur, enabling learning-based pipelines that map event streams to relevant structure and control signals (Kim et al., 2016; Liu et al., 2025). This line is promising for fast, cluttered, and high-contrast scenes, but standardized event benchmarks and task-specific architectures for 6-DoF grasping remain limited.

2.3 SPIKE CAMERA APPLICATIONS

Many works around spike cameras have been created recently. Image reconstruction is a popular topic among these works. Zhu (Zhu et al., 2019) reconstruct images with the count of spikes and the spike intervals, respectively. Subsequent methods reconstruct images from spikes with filtering (Dong et al., 2022), neuron models (Zheng et al., 2021), optimization (Zhao et al., 2021c), and deep neural networks (Zhao et al., 2021b). MGSR (Zhao et al., 2021a), SpikeSRNet (Zhao et al., 2023), and Xiang (Xiang et al., 2021) estimate super-resolved images from spikes based on the fusion of multi-frames. Han (Han et al., 2020) and Zhou (Zhou et al., 2020) use spike cameras to perform high dynamic range imaging. Xia (Xia et al., 2023) uses spikes to assist video frame interpolation. Besides getting images, various tasks have been developed. Zhu (Zhu et al., 2022) and Li (Li et al., 2022) propose object detection methods based on spike streams. SCFlow (Hu et al., 2022) estimates the optical flow directly from the binary spike streams based on a pyramidal network. The Spike Transformer (Zhang et al., 2022) estimates the depth of the spike camera with the transformer.

3 METHOD

We introduce our end-to-end 6-DoF pose detection network based stereo spike streams, which are illustrated in Fig. 2. The grasp pose representation is introduced in Section 3.2. We divide our pipeline into three parts: Visual Pathway Network, Graspable Network and Grasp Detection Network.

3.1 PRELIMINARY OF THE SPIKE CAMERA

The spike camera emulates the retinal fovea with an integrate-and-fire architecture. Each pixel contains a photoreceptor, an integrator, and a comparator. Photons are first converted to charge, which the integrator accumulates. When the accumulated value exceeds a threshold θ , the pixel emits a binary event, and the integrator resets. The pixels operate independently, yielding fully asynchronous sensing, while the array is read out synchronously at up to 40,000 Hz. For a pixel at the location (x, y) , the accumulated charge is:

$$A(x, y, t) = \left(\int_0^t I(x, y, s) ds \right) \bmod \theta, \quad (1)$$

where $I(x, y, s)$ is the incident irradiance. The modulo term guarantees at most one spike per readout interval. Capturing a scene for a duration T produces a spike tensor $S \in \{0, 1\}^{K \times H \times W}$ with K binary frames, and H and W represent the height and width, respectively, whose event density encodes the underlying luminance dynamics.

3.2 GRASP POSE REPRESENTATION

Similarly to previous work, we attached a local coordinate frame to the two-finger parallel gripper. A grasp in the camera frame is defined by orientation $\mathbf{R} \in \mathbb{R}^{3 \times 3}$, translation $\mathbf{t} \in \mathbb{R}^{3 \times 1}$, and a tight

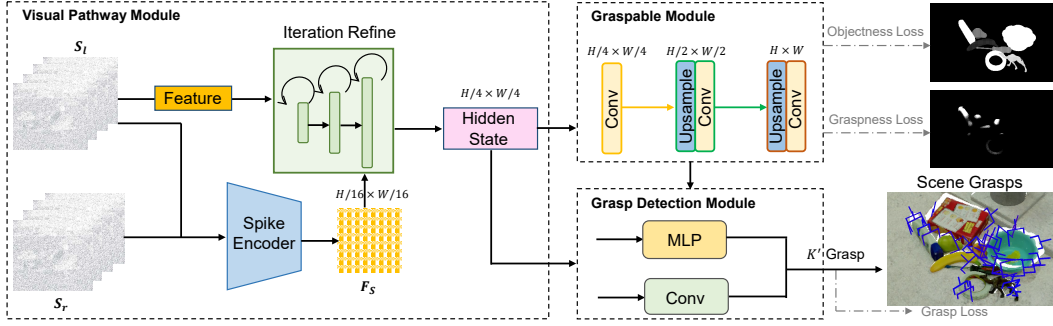


Figure 2: Overview of SpikeGrasp, the method for direct 6D grasp pose detection from raw stereo spike streams. First, left and right features are extracted from the spike streams to construct correlation features. This correlation feature is fed into an iterative refinement network along with spike features to predict the hidden state of the original 1/4 resolution. Then these hidden states are input into a graspable network (multi-layer convolution and upsampling structure), which uses the raw data as supervision to predict the objectness and graspness of the grasping scene, and these states collectively form the object-scene graspable information. Finally, the obtained hidden states and graspable information are input into the grasp detection network, and the grasp scores and gripper widths are predicted for each group and used to output K' grasp poses.

gripper width $w \in \mathbb{R}$, written as

$$\mathbf{G} = (\mathbf{R}, \mathbf{t}, w), \quad (2)$$

and directly regressing the full rotation matrix is unstable because the network must satisfy orthogonality and unit determinant constraints. Instead, we adopt the 6D pose parameterization, which decomposes \mathbf{R} into a discrete viewpoint class and a continuous rotation of the in-plane. Thus, for each surface point the network predicts: (i) a feasible approach vector, (ii) the approach distance, (iii) the rotation about this vector, and (iv) a tight gripper width. This compact representation is easier to learn and produces mechanically valid grasp poses.

3.3 VISUAL PATHWAY NETWORK

This subsection describes architectures of the Visual Pathway Network. It illustrates the biologically inspired framework design, where stereo spike signals from both cameras are processed through a context network. Correlation features are computed and temporally refined via recurrent spiking neural network (RSNN) blocks. The network consists of three main components: a multi-scale spike feature extractor, a correlation volume module, and a biologically inspired update operator.

3.3.1 SPIKE FEATURE EXTRACTION

Given left and right spike streams $S_l, S_r \in \mathbb{R}^{N \times H \times W}$, we first apply a 7×7 convolution with stride 2 to obtain half-resolution representations. These activations pass through a stack of residual blocks that refine the temporal and spatial correlations. A second downsampling layer produces 1/4-resolution feature maps $f_{l,4}, f_{r,4} \in \mathbb{R}^{C_4 \times H/4 \times W/4}$, which are used to build the cost volume. To guide subsequent 3D regularization, we further derive multi-scale features.

$$\{f_{l,i}, f_{r,i} \in \mathbb{R}^{C_i \times H_i \times W_i} \mid i \in \{4, 8, 16\}\}, \quad (3)$$

where C_i is fixed to 128.

3.3.2 CORRELATION VOLUME

Given left and right feature maps $f^l, f^r \in \mathbb{R}^{C \times H \times W}$, we measure similarity along the hidden state by computing an all-pairs correlation:

$$\mathbf{C}_{i,j,k} = \sum_h f_{h,i,j}^l f_{h,i,k}^r, \mathbf{C} \in \mathbb{R}^{H/4 \times W/4 \times W/4}, \quad (4)$$

and the resulting tensor $C \in \mathbb{R}^{D \times H \times W}$ forms the initial cost volume. To capture context at multiple resolutions, we build a four-level correlation pyramid $\{C^{(1)}, \dots, C^{(4)}\}$ by successively applying 1D average pooling along the dimension with kernel size 2 and stride 2. Each level halves the resolution while preserving spatial dimensions, enabling coarse to fine matching in subsequent stages.

3.3.3 ITERATIVE UPDATE

We maintain a single hidden state field h that encodes both visible and occluded geometry. In iteration k , we sample the cost features of the correlation pyramid at resolutions of 1/8, 1/16, and 1/32, conditioned on the current state h^k . These multi-scale features, together with spike context cues S_c , are passed to a three-layer RSNN-based update module that shares weights across scales and exchanges hidden activations between resolutions. The module predicts an increment Δh and a refreshed state, and we update the field by

$$h^{k+1} = h^k + \Delta h. \quad (5)$$

Operating across coarse-to-fine grids rapidly enlarges the receptive field, improving robustness in large texture-poor regions, while final correlation lookup and refinement are performed at the highest resolution to preserve detail.

3.3.4 SPIKE OUTPUT

The output spikes s_t are sequentially fed into the SNN decoder, which outputs spike trains $s_T \in \{0, 1\}^{B \times T \times H \times W}$. We need to decode them into the hidden state $h_T \in \mathbb{R}^{B \times T \times H \times W}$. Using the RSNN framework, we employ the membrane potentials of output neurons to perform spike-to-hidden-state decoding. We use spiking neurons in the output layer and convert s_T into real values by measuring the membrane potential at the final time step T . This is given by the following equation:

$$\begin{aligned} v_T^{\text{out}} &= \tau_{\text{out}} v_{T-1}^{\text{out}} + s_T \\ &= \sum_{t=1}^T \tau_{\text{out}}^{T-t} s_t \end{aligned} \quad (6)$$

We set $\tau_{\text{out}} = 0.9$, and we obtain the real-valued reconstructed as $h_T = \text{ReLU}(v_T^{\text{out}})$.

3.4 GRASPABLE NETWORK

The final hidden state h^K is decoded by multi-layer convolutional networks and upsampling layers to produce a two-channel probability map $M \in \mathbb{R}^{2 \times H \times W}$. The first channel, objectness, gives a per-pixel likelihood that a pixel belongs to any foreground object, while the second channel, graspness, scores how suitable that pixel is for a gripper contact according to local geometric cues.

The network adopts an encoder-decoder topology with skip connections to preserve fine details. Each encoder stage applies two 3×3 convolutions followed by ReLU and downsampling, and the decoder mirrors this structure, using bilinear upsampling and concatenating features from the corresponding encoder stage. A final 1×1 convolution reduces the feature dimension to two, and a sigmoid activation converts logits to probabilities. During training, the model was encouraged to highlight graspable regions even in cluttered scenes.

3.5 GRASP DETECTION NETWORK

From the final hidden state h^K and a set of graspable locations, the Grasp Detection Network predicts complete 6-DoF grasp configurations. Each grasp is defined by a view vector, approach depth, in-plane rotation, gripper width, and a confidence score. We adopt a crop-and-refine strategy. For each of the M seed location-view pairs, a directional cylindrical region is carved out with height d and radius r . The coordinates inside the cylinder are transformed into the canonical gripper frame, normalized by r , and concatenated with the corresponding hidden features, producing candidate tensors of shape $M \times K \times (3 + C)$, where K is the number of samples per region and C the feature dimension. A shared set encoder built from multilayer perceptrons followed by a max-aggregation layer compresses each candidate to a feature vector of dimension C' . The final prediction head outputs, for each candidate, scores and widths across A discretized in-plane rotations and D approach depths, resulting in an output tensor of size $M \times (A \times D \times 2)$.

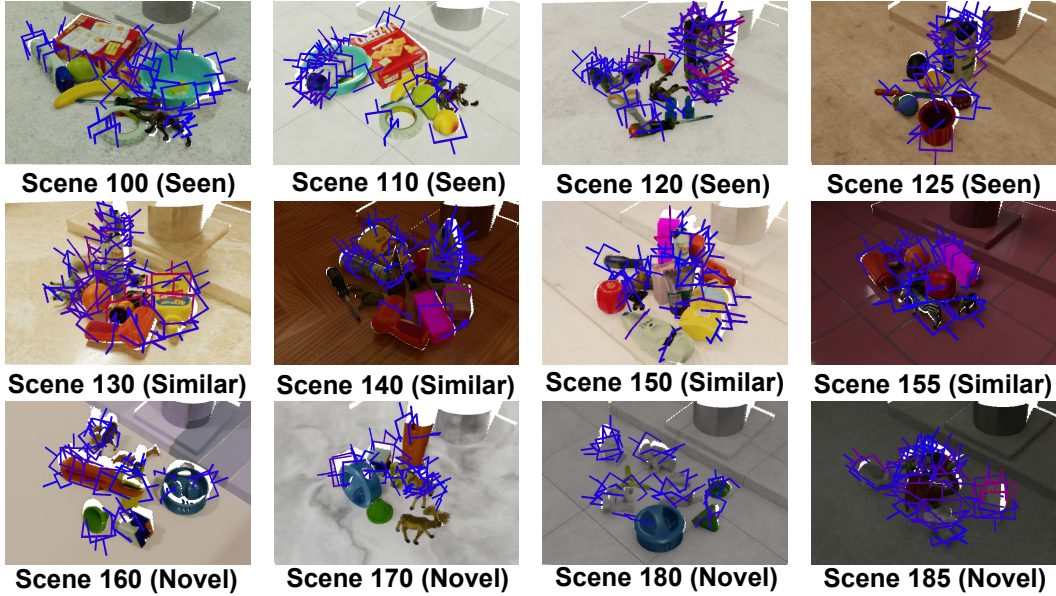


Figure 3: Visualizations of the top 50 grasp poses predicted by our SpikeGrasp algorithm from 12 different scenes (four scenes per subset). A gripper-shaped geometry represents the grasp pose. The grasp pose color changes from blue to purple to indicate increasing confidence.

The grasp with the highest score is selected as the final estimate. By combining multi-scale sampling, canonical alignment, and weight sharing, the network efficiently explores the grasp space while preserving geometric consistency.

3.5.1 GRASP SCORE REPRESENTATION

We quantify grasp quality by the minimum friction coefficient u_i that guarantees force closure. A lower u_i implies a stronger grasp. To convert u_i into normalized confidence, the method we use is defined similarly to GSNNet (Wang et al., 2021), as follows:

$$q_i = \begin{cases} \frac{\ln(u_{\max}/u_i)}{\ln(u_{\max}/u_{\min})}, & \text{if the grasp is positive,} \\ 0, & \text{others,} \end{cases} \quad (7)$$

where u_{\min} and u_{\max} are empirical lower and upper bounds. This mapping yields scores $q_i \in [0, 1]$: $q_i = 1$ for the most stable grasps ($u_i \rightarrow u_{\min}$) and $q_i = 0$ for infeasible candidates.

3.6 LOSS FUNCTION

The network is training with a multi-task loss, and the main parameter settings in loss are derived from (Wang et al., 2021), as follows:

$$L = L_{obj} + \alpha(L_p + \lambda L_v) + \beta(L_s + L_w), \quad (8)$$

where L_{obj} is the classification that supervises the per-pixel objectness map, L_p and L_v regress the point-wise and view-wise graspable landscapes, and L_s and L_w are the grasp scores and gripper widths, respectively. The terms L_p and L_s are evaluated only in locations identified as belonging to objects, L_v is applied to predefined seed views, and L_w is computed for grasp hypotheses whose ground-truth scores are positive. The weighting factors α , β , and λ balance the influence of coverage, viewpoint reasoning, quality estimation, and gripper configuration during training. We use softmax for classification tasks and smooth- l_1 loss for regression tasks.

Table 1: Quantitative evaluation of grasp pose prediction on the synthetic dataset. Similar to the other baseline methods, we report the average precision (AP), $AP_{0.4}$, and $AP_{0.8}$. Note that 0.4 and 0.8 denote the friction coefficients, and the lower the more difficult. O and G in the output column indicate whether the objectness and graspness modules are used, respectively.

Method	Output		Seen			Similar			Novel		
	O	G	AP	$AP_{0.8}$	$AP_{0.4}$	AP	$AP_{0.8}$	$AP_{0.4}$	AP	$AP_{0.8}$	$AP_{0.4}$
GG-CNN			15.48	21.84	10.25	13.26	18.37	4.62	5.52	5.93	1.86
ASGrasp			16.89	22.47	11.23	15.05	19.76	6.19	7.38	8.78	1.32
GraspARL	✓		15.97	23.66	10.80	15.41	20.21	7.06	7.64	8.69	2.52
GraspNet	✓		27.56	33.43	16.59	26.11	34.18	14.23	10.55	11.25	3.98
CenterGrasp			16.46	20.24	11.74	9.52	11.92	5.71	1.60	1.89	1.12
GraspNeRF			22.87	28.53	12.84	21.33	27.83	9.64	8.24	8.89	2.67
GNet	✓	✓	34.52	48.36	20.80	30.11	36.22	18.71	14.11	20.52	14.23
KGNv2	✓		25.96	33.01	15.37	22.68	29.15	10.76	9.23	9.89	2.74
GraspFast	✓		38.46	44.25	28.66	33.83	40.05	21.32	14.63	21.05	12.85
SpikeGrasp (Ours)	✓	✓	38.84	47.27	29.57	34.84	40.32	25.48	15.39	18.09	9.80

4 EXPERIMENTS

4.1 BENCHMARK DATASET

We construct a synthetic dataset for spike-based 6-DoF grasp learning in Blender (Community, 2018). The dataset comprises 190 scenes, split into 100 for training and 90 for testing, and the test set is further divided into 30 scenes with previously seen objects, 30 with unseen yet similar objects, and 30 with novel objects to test generalization. Each scene contains 255 pairs of spike streams with ground-truth masks. Using 88 object models (Fang et al., 2020), we applied physics-based simulation and extensive domain randomization lighting, pose, and camera viewpoint to produce physically plausible images. The dataset statistics, methods for the generation of dense spike streams with high temporal resolution, and other analyzes follow the protocol are provided in the Appendix A.3.

4.2 TRAINING AND INFERENCE

Our model is implemented with PyTorch and trained on Nvidia RTX 4090 GPUs for 18 epochs with Adam optimizer and the batch size of 4. The learning rate is 2×10^{-4} in the first epoch and multiplied by 0.95 every epoch. During training, we apply 16 update iterations for each sample, use one GPU for model updating, and one GPU for label generation. In inference, we only use one GPU for fast prediction.

4.3 COMPARABLE EXPERIMENTS

We compare our method with previous representative methods and the comparison models are as follows. GG-CNN (Morrison et al., 2018) predicts planar grasp rectangles from RGB spikes, while GraspARL (Wu et al., 2022) and CenterGrasp (Chisari et al., 2024) classify heuristic grasp samples generated from depth images. GraspNet (Fang et al., 2020), GNet (Wang et al., 2021), GraspFast (Gui et al., 2025) and KGNv2 (Chen et al., 2023) serve as an end-to-end 6-DoF baseline operating directly on depth input. ASGrasp (Shi et al., 2024) and GraspNeRF (Dai et al., 2022b) directly estimate the grasp pose from multiple RGB images.

We trained all models in the synthetic training dataset and evaluated three test subsets which are seen, similar, and novel objects. As shown in Table 1, SpikeGrasp achieves the highest accuracy in most subsets without post-processing, especially evident in the Seen and Similar subsets. Qualitative comparisons in Fig. 3 confirm these gains: top-1 grasp success with spike input reaches 78.53%, 72.18%, and 36.79% for the three subsets, respectively. This result supports the importance and feasibility of robot grasping from large-scale grasp pose datasets and raw spike streams.

To visually illustrate the outstanding performance of our proposed SpikeGrasp algorithm in 6-DoF grasp pose detection, we performed a comparative visualization among our algorithms, as shown in Fig. 3. Four scenes are randomly sampled from each test segment for inspection. Across all cases, SpikeGrasp assigns higher confidence to its top-50 grasp proposals and, unlike GraspNet, covers a

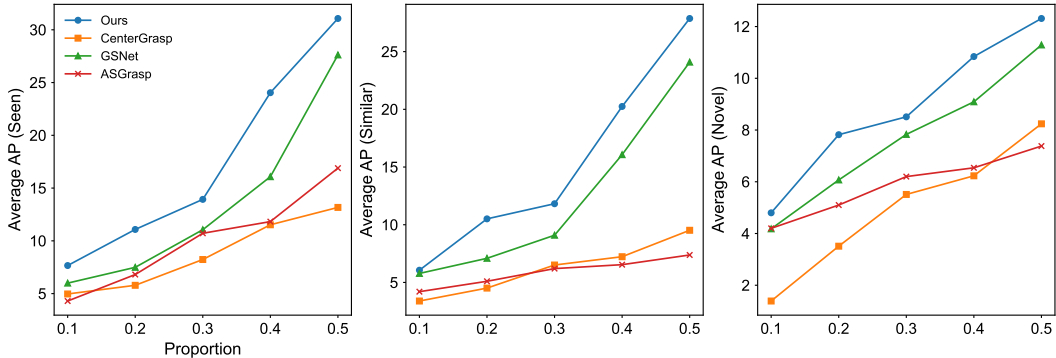


Figure 4: Data efficiency experiments on the synthetic dataset. The horizontal axis indicates the proportion of the training set, while the vertical axes represent the value of AP.

broader range of object categories. Compared with ASGrasp, it also yields more intuitive, object-aligned poses. For instance, in scene 130, all SpikeGrasp proposals correctly land on object surfaces. These observations indicate that SpikeGrasp offers more reliable and precise grasp hypotheses in cluttered environments while maintaining wider object coverage. More visual results can be found in the Appendix A.4.

4.4 DATA EFFICIENCY

To assess data efficiency, we trained our model and all baselines in randomly sampled subsets of the synthetic training set, ranging from 50% down to 10% in 10% increments—while evaluating on the full test set for fair comparison. As shown in Fig. 4, our method consistently exceeds all baselines at every training ratio, with margins widening as data become scarcer. This indicates a stronger generalization under limited supervision and highlights the robustness and data efficiency of the learned representations.

4.5 COMPUTATIONAL COST

In our model, the iterative refinement process uses a three-layer RSNN, so we count the floating-point (FP) additions and multiplications required to infer a single grasp. In ANNs, each MAC entails one FP multiplication and one FP addition; in binary-spike SNNs, only FP additions are triggered, and time steps without spikes incur no computation. We report an operation-weighted complexity ratio based on per-operation weights w_{MAC} and w_{AC} (reflecting the higher cost of multiplications compared to additions):

$$\frac{C_{SNN}}{C_{ANN}} = \frac{N_{MAC}^{SNN} w_{MAC} + N_{AC}^{SNN} w_{AC}}{N_{MAC}^{ANN} w_{MAC}}. \quad (9)$$

Here, $N_{(\cdot)}^{(\cdot)}$ denotes the total number of operations, with subscripts AC (accumulation) or MAC (multiply-accumulate) and superscripts indicating the type of network (ANN or SNN), and we set $w_{MAC} = 4.6$ and $w_{AC} = 0.9$ (Huang et al., 2025). Furthermore, since our inputs are the spike streams, we can estimate $N_{MAC}^{SNN} \approx 0$. We evaluated the computational cost ratio of this module as well as its ratio to an ANN with the same number of neurons, along with the counts of floating-point additions and multiplications. The results are shown in Table 2.

In general, the RSNN reduces the total FP operation count by 2.3 times relative to the ANN; since multiplications dominate cost, cutting them is especially beneficial. Moreover, RSNNs are expected to run over two orders of magnitude faster than ANNs on neuromorphic hardware, indicating substantial speedups alongside the reduced FP operation load. In summary, SNN-based SpikeGrasp achieves significant computation savings (a reduction 82.5%) through sparsity, highlighting the need for hardware advancements to support longer integration times.

Model	Computational complexity		Ratio
	Addition	Multiplication	
ANN	1.6×10^{10}	1.6×10^{10}	1
RSNN (Ours)	2.8×10^{10}	0	0.175

Table 2: Comparison of the computational cost required to infer a single grasp pose detection. The computational consumption of ANN with the same number of neurons is taken as 1.

Model	Grasp Pose		
	Seen	Similar	Novel
w/o objectness	26.14	24.41	5.54
w/o graspness	34.78	30.86	11.28
w/o objectness + graspness	15.85	12.08	4.43
w/o spike	25.86	24.84	8.59
w/o adaptive variables	21.87	19.33	7.24
Ours (default)	38.84	34.84	15.39

Table 3: Ablation studies on the network input, architecture, and algorithm. For grasp pose prediction, we report the metrics AP of the synthetic dataset.

4.6 ABLATION STUDY

To evaluate the effectiveness of different components in our network, we performed ablation studies on the dataset. Firstly, we evaluate the effectiveness of the objectness and graspness modules by removing each module separately from the inference pipeline. Then, we removed the structures in the stereo network by replacing the RSNN structure used for iterative refinement updates with an RNN structure containing the same number of neurons, i.e., removing the spike input from the network. The second is to use LIF neurons with the same number as adaptive LIF neurons and remove adaptive variables from the neurons. Under the same training parameters, the networks with the above modifications were re-trained and tested, and the results are shown in Table 3.

We observe that performance degradation after removing the objectness or graspness module demonstrates the effectiveness of the graspable regions driven by the graspable network in the grasping process. Meanwhile, when iteration modules are replaced or the dynamics of neurons within the visual pathway network are changed, the performance of the network drops, confirming that these components are critical for modeling grasp-affinity fields in our framework.

4.7 SIMULATION EVALUATION

We evaluated feasibility and generalization in NVIDIA Isaac Sim using a Franka Emika Panda with a Robotiq 2F-85 gripper. We instantiate 15 tabletop scenes, each containing 6-8 objects drawn directly from our synthetic dataset object files. For each object, we conduct repeated pick attempts with a maximum of three trials. A grasp is counted as successful if the object is lifted and held stably after closure. Trained only on synthetic data, our model achieved success rates of 91.3%, 85.8%, and 70.9% in the Seen, Similar, and Novel datasets, respectively. These results demonstrate a strong transfer from the synthetic environment to the simulation and confirm the robustness of our approach. Additional setup details and qualitative expansion are provided in the Appendix A.4.

5 CONCLUSION

In this paper, we propose SpikeGrasp, a first state-of-the-art deep learning framework for 6-DoF grasp pose detection from raw spike streams of spike cameras without depth or point cloud. It features a biologically plausible update operator based on a spike feature extraction and a stereo network, and our extensive analysis confirms the effectiveness of these components. Additionally, we have constructed a synthetic stereo spike stream dataset with corresponding grasp labels and

we believe that this dataset will facilitate future research on robotic grasping using spike cameras. Overall, SpikeGrasp represents an advancement in neuromorphic stereo vision and demonstrates the potential of spike-based systems in 3D perception and embodied intelligence.

Limitations. Our experiments are based on a synthetic dataset in which input, scene, and segmentation labels are generated by a simulator, while 6-DoF grasp annotations of objects are sourced from GraspNet-1Billion. Although the model performs well in simulation, its effectiveness is constrained by the domain gap between synthetic and real data, and current training does not fully bridge this distribution shift. We plan to reduce this gap, e.g., collecting real spike streams with paired annotations, exploring hybrid domain transfer, and weakly supervised fine-tuning on real-world scenes.

ETHICS STATEMENT

This study complies with the Code of Ethics. No human subject data or personally identifiable information was used; all experiments are based on publicly available datasets released under permissive licenses and self-built datasets. We provide complete documentation, code, and random seeds to facilitate reproducibility and prevent research misconduct. The proposed method is intended for general scientific research. There are no conflicts of interest or harmful applications beyond the stated scope.

REPRODUCIBILITY STATEMENT

We commit to reproducibility by releasing an anonymized codebase with configuration files, pinned dependencies, and scripts for training, evaluation, and figure/table generation. The main paper outlines the model and algorithms, while the Appendix details architectures, hyperparameters, optimizer schedules, random seeds, and computational budgets. For theoretical results, all assumptions and complete proofs are provided in the Appendix. All datasets and splits are described in the Supplementary, including preprocessing pipelines and data generation steps. We also include instructions for environment setup (e.g., Conda/requirements) and links to pretrained checkpoints. We are about to release our datasets and code repository.

REFERENCES

- Michel Breyer, Jen Jen Chung, Lionel Ott, Roland Siegwart, and Juan Nieto. Volumetric grasping network: Real-time 6 dof grasp detection in clutter. In *Conference on robot learning*, pp. 1602–1611. PMLR, 2021.
- Sheng-Hao Cao, Xin-Yong Han, Zhi-Ping Zhao, Jian-Wen Gu, Tian-Zi Jiang, and Shan Yu. Hand position fields of neurons in the premotor cortex of macaques during natural reaching. *Nature Communications*, 16(1):3489, 2025.
- Siang Chen, Wei Tang, Pengwei Xie, Wenming Yang, and Guijin Wang. Efficient heatmap-guided 6-dof grasp detection in cluttered scenes. *arXiv preprint arXiv:2403.18546*, 2024.
- Yiye Chen, Ruinian Xu, Yunzhi Lin, Hongyi Chen, and Patricio A Vela. Kgnv2: Separating scale and pose prediction for keypoint-based 6-dof grasp synthesis on rgb-d input. In *2023 IEEE/RSJ International Conference on Intelligent Robots and Systems (IROS)*, pp. 2971–2978. IEEE, 2023.
- Eugenio Chisari, Nick Heppert, Tim Welschhold, Wolfram Burgard, and Abhinav Valada. Center-grasp: Object-aware implicit representation learning for simultaneous shape reconstruction and 6-dof grasp estimation. *IEEE Robotics and Automation Letters*, 9(6):5094–5101, 2024.
- Community. Blender - a 3d modelling and rendering package, 2018. <http://www.blender.org>.
- Qiyu Dai, Jiyao Zhang, Qiwei Li, Tianhao Wu, Hao Dong, Ziyuan Liu, Ping Tan, and He Wang. Domain randomization-enhanced depth simulation and restoration for perceiving and grasping specular and transparent objects. In *European Conference on Computer Vision*, pp. 374–391. Springer, 2022a.

-
- Qiyu Dai, Yan Zhu, Yiran Geng, Ciyu Ruan, Jiazhao Zhang, and He Wang. Graspnerf: Multiview-based 6-dof grasp detection for transparent and specular objects using generalizable nerf. *arXiv preprint arXiv:2210.06575*, 2022b.
- Xinke Deng, Yu Xiang, Arsalan Mousavian, Clemens Eppner, Timothy Bretl, and Dieter Fox. Self-supervised 6d object pose estimation for robot manipulation. In *2020 IEEE International Conference on Robotics and Automation (ICRA)*, pp. 3665–3671. IEEE, 2020.
- Y. Dong, J. Zhao, R. Xiong, and T. Huang. 3D residual interpolation for spike camera demosaicing. In *Proceedings of the IEEE International Conference on Image Processing (ICIP)*, pp. 1461–1465, 2022.
- Hao-Shu Fang, Chenxi Wang, Minghao Gou, and Cewu Lu. Graspnet-1billion: A large-scale benchmark for general object grasping. In *Proceedings of the IEEE/CVF conference on computer vision and pattern recognition*, pp. 11444–11453, 2020.
- Hao-Shu Fang, Chenxi Wang, Hongjie Fang, Minghao Gou, Jirong Liu, Hengxu Yan, Wenhai Liu, Yichen Xie, and Cewu Lu. Anygrasp: Robust and efficient grasp perception in spatial and temporal domains. *IEEE Transactions on Robotics*, 39(5):3929–3945, 2023.
- Minghao Gou, Hao-Shu Fang, Zhanda Zhu, Sheng Xu, Chenxi Wang, and Cewu Lu. Rgb matters: Learning 7-dof grasp poses on monocular rgbd images. In *2021 IEEE International Conference on Robotics and Automation (ICRA)*, pp. 13459–13466. IEEE, 2021.
- Haiyuan Gui, Shanchen Pang, Xiao He, Luqi Wang, Xue Zhai, Shihang Yu, and Kuijie Zhang. Graspfast: Multi-stage lightweight 6-dof grasp pose fast detection with rgb-d image. *Pattern Recognition*, 161:111318, 2025.
- J. Han, C. Zhou, P. Duan, Y. Tang, C. Xu, C. Xu, T. Huang, and B. Shi. Neuromorphic camera guided high dynamic range imaging. In *Proceedings of the IEEE/CVF Conference on Computer Vision and Pattern Recognition (CVPR)*, pp. 1730–1739, 2020.
- Dinh-Cuong Hoang, Johannes A Stork, and Todor Stoyanov. Context-aware grasp generation in cluttered scenes. In *2022 International Conference on Robotics and Automation (ICRA)*, pp. 1492–1498. IEEE, 2022.
- L. Hu, R. Zhao, Z. Ding, L. Ma, B. Shi, R. Xiong, and T. Huang. Optical flow estimation for spiking camera. In *Proceedings of the IEEE/CVF Conference on Computer Vision and Pattern Recognition (CVPR)*, 2022.
- Zihan Huang, Wei Fang, Tong Bu, Peng Xue, Zecheng Hao, Wenxuan Liu, Yuanhong Tang, Zhaofei Yu, and Tiejun Huang. Differential coding for training-free ann-to-snn conversion. *arXiv preprint arXiv:2503.00301*, 2025.
- Shun Iwase, Muhammad Zubair Irshad, Katherine Liu, Vitor Guizilini, Robert Lee, Takuya Ikeda, Ayako Amma, Koichi Nishiwaki, Kris Kitani, Rares Ambrus, et al. Zerograsp: Zero-shot shape reconstruction enabled robotic grasping. In *Proceedings of the Computer Vision and Pattern Recognition Conference*, pp. 17405–17415, 2025.
- Snehal Jauhri, Ishikaa Lunawat, and Georgia Chalvatzaki. Learning any-view 6dof robotic grasping in cluttered scenes via neural surface rendering. *arXiv preprint arXiv:2306.07392*, 2023.
- Hanme Kim, Stefan Leutenegger, and Andrew J Davison. Real-time 3d reconstruction and 6-dof tracking with an event camera. In *European conference on computer vision*, pp. 349–364. Springer, 2016.
- J. Li, X. Wang, L. Zhu, J. Li, T. Huang, and Y. Tian. Retinomorph object detection in asynchronous visual streams. In *Proceedings of the AAAI Conference on Artificial Intelligence*, pp. 1332–1340, 2022.
- Hongzhuo Liang, Xiaojian Ma, Shuang Li, Michael Görner, Song Tang, Bin Fang, Fuchun Sun, and Jianwei Zhang. Pointnetgpd: Detecting grasp configurations from point sets. In *2019 International Conference on Robotics and Automation (ICRA)*, pp. 3629–3635. IEEE, 2019.

-
- Tsung-Yi Lin, Michael Maire, Serge Belongie, James Hays, Pietro Perona, Deva Ramanan, Piotr Dollár, and C Lawrence Zitnick. Microsoft coco: Common objects in context. In *European conference on computer vision*, pp. 740–755. Springer, 2014.
- Xiaozheng Liu, Yunzhou Zhang, He Cao, Dexing Shan, and Jiaqi Zhao. Joint segmentation and grasp pose detection with multi-modal feature fusion network. In *2023 IEEE International Conference on Robotics and Automation (ICRA)*, pp. 1751–1756. IEEE, 2023.
- Zibin Liu, Banglei Guan, Yang Shang, Yifei Bian, Pengju Sun, and Qifeng Yu. Stereo event-based, 6-dof pose tracking for uncooperative spacecraft. *IEEE Transactions on Geoscience and Remote Sensing*, 2025.
- Jeffrey Mahler, Jacky Liang, Sherdil Niyaz, Michael Laskey, Richard Doan, Xinyu Liu, Juan Aparicio Ojea, and Ken Goldberg. Dex-net 2.0: Deep learning to plan robust grasps with synthetic point clouds and analytic grasp metrics. *arXiv preprint arXiv:1703.09312*, 2017.
- Douglas Morrison, Peter Corke, and Jürgen Leitner. Closing the loop for robotic grasping: A real-time, generative grasp synthesis approach. *arXiv preprint arXiv:1804.05172*, 2018.
- Peiyuan Ni, Wenguang Zhang, Xiaoxiao Zhu, and Qixin Cao. Pointnet++ grasping: Learning an end-to-end spatial grasp generation algorithm from sparse point clouds. In *2020 IEEE International Conference on Robotics and Automation (ICRA)*, pp. 3619–3625. IEEE, 2020.
- Ran Qin, Haoxiang Ma, Boyang Gao, and Di Huang. Rgb-d grasp detection via depth guided learning with cross-modal attention. *arXiv preprint arXiv:2302.14264*, 2023.
- Yuzhe Qin, Rui Chen, Hao Zhu, Meng Song, Jing Xu, and Hao Su. S4g: Amodal single-view single-shot se (3) grasp detection in cluttered scenes. In *Conference on robot learning*, pp. 53–65. PMLR, 2020.
- Jun Shi, A Yong, Yixiang Jin, Dingzhe Li, Haoyu Niu, Zhezhu Jin, and He Wang. Asgrasp: Generalizable transparent object reconstruction and grasping from rgb-d active stereo camera. *CoRR*, 2024.
- Martin Sundermeyer, Arsalan Mousavian, Rudolph Triebel, and Dieter Fox. Contact-graspnet: Efficient 6-dof grasp generation in cluttered scenes. In *2021 IEEE International Conference on Robotics and Automation (ICRA)*, pp. 13438–13444. IEEE, 2021.
- Andreas Ten Pas, Marcus Gualtieri, Kate Saenko, and Robert Platt. Grasp pose detection in point clouds. *The International Journal of Robotics Research*, 36(13-14):1455–1473, 2017.
- Chenxi Wang, Hao-Shu Fang, Minghao Gou, Hongjie Fang, Jin Gao, and Cewu Lu. Graspness discovery in clutters for fast and accurate grasp detection. In *Proceedings of the IEEE/CVF International Conference on Computer Vision*, pp. 15964–15973, 2021.
- Tianhao Wu, Fangwei Zhong, Yiran Geng, Hongchen Wang, Yongjian Zhu, Yizhou Wang, and Hao Dong. Graspnet: Dynamic grasping via adversarial reinforcement learning. *arXiv preprint arXiv:2203.02119*, 2022.
- L. Xia, J. Zhao, R. Xiong, and T. Huang. SVFI: Spiking-based video frame interpolation for high-speed motion. In *Proceedings of the AAAI Conference on Artificial Intelligence*, pp. 2910–2918, 2023.
- X. Xiang, L. Zhu, J. Li, Y. Wang, T. Huang, and Y. Tian. Learning super-resolution reconstruction for high temporal resolution spike stream. *IEEE Transactions on Circuits and Systems for Video Technology*, 2021.
- Christopher Xie, Yu Xiang, Arsalan Mousavian, and Dieter Fox. Unseen object instance segmentation for robotic environments. *IEEE Transactions on Robotics*, 37(5):1343–1359, 2021.
- J. Zhang, L. Tang, Z. Yu, J. Lu, and T. Huang. Spike transformer: Monocular depth estimation for spiking camera. In *Proceedings of the European Conference on Computer Vision (ECCV)*, 2022.

-
- Jiyao Zhang, Weiyao Huang, Bo Peng, Mingdong Wu, Fei Hu, Zijian Chen, Bo Zhao, and Hao Dong. Omni6dpose: A benchmark and model for universal 6d object pose estimation and tracking. In *European Conference on Computer Vision*, pp. 199–216. Springer, 2024.
- J. Zhao, J. Xie, R. Xiong, J. Zhang, Z. Yu, and T. Huang. Super resolve dynamic scene from continuous spike streams. In *Proceedings of the IEEE/CVF International Conference on Computer Vision (ICCV)*, pp. 2533–2542, 2021a.
- J. Zhao, R. Xiong, H. Liu, J. Zhang, and T. Huang. Spk2ImgNet: Learning to reconstruct dynamic scene from continuous spike stream. In *Proceedings of the IEEE/CVF Conference on Computer Vision and Pattern Recognition (CVPR)*, pp. 11996–12005, 2021b.
- J. Zhao, R. Xiong, J. Xie, B. Shi, Z. Yu, W. Gao, and T. Huang. Reconstructing clear image for high speed motion scene with a retina-inspired spike camera. *IEEE Transactions on Computational Imaging*, 8:12–27, 2021c.
- J. Zhao, R. Xiong, J. Zhang, R. Zhao, H. Liu, and T. Huang. Learning to super-resolve dynamic scenes for neuromorphic spike camera. In *Proceedings of the AAAI Conference on Artificial Intelligence*, pp. 3579–3587, 2023.
- Y. Zheng, L. Zheng, Z. Yu, B. Shi, Y. Tian, and T. Huang. High-speed image reconstruction through short-term plasticity for spiking cameras. In *Proceedings of the IEEE/CVF Conference on Computer Vision and Pattern Recognition (CVPR)*, pp. 6358–6367, 2021.
- Yajing Zheng, Jiyuan Zhang, Rui Zhao, Jianhao Ding, Shiyan Chen, Ruiqin Xiong, Zhaofei Yu, and Tiejun Huang. Spikecv: open a continuous computer vision era. *arXiv preprint arXiv:2303.11684*, 2023.
- C. Zhou, H. Zhao, J. Han, C. Xu, C. Xu, T. Huang, and B. Shi. Unmodnet: Learning to unwrap a modulo image for high dynamic range imaging. In *Advances in Neural Information Processing Systems (NeurIPS)*, pp. 1559–1570, 2020.
- L. Zhu, S. Dong, T. Huang, and Y. Tian. A retina inspired sampling method for visual texture reconstruction. In *Proceedings of the IEEE International Conference on Multimedia and Expo (ICME)*, pp. 1432–1437, 2019.
- Y. Zhu, Y. Zhang, X. Xie, and T. Huang. An FPGA accelerator for high-speed moving objects detection and tracking with a spike camera. *Neural Computation*, 34(8):1812–1839, 2022.

A APPENDIX

The appendix provides additional implementation details and extended experimental results for the SpikeGrasp framework introduced in the main paper. It is organized into four distinct sections: The Use of Large Language Models in Appendix A.1, Theory Analysis and Method in Appendix A.2, Details of the Dataset in Appendix A.3, More Experimental Results in Appendix A.4 and Broader Impacts in Appendix A.5.

A.1 THE USE OF LARGE LANGUAGE MODELS (LLMs)

We use LLMs only for grammar and style polishing, not for generating technical content, and no proprietary data or restricted code are shared with them. The authors bear full responsibility for the content of the paper.

A.2 THEORY ANALYSIS AND METHOD

A.2.1 PROBLEM STATEMENT

Given a continuous binary spike stream $S_N^{t_1} \in \{0, 1\}^{H \times W \times N}$ with a spatio-temporal resolution of $H \times W \times N$, centered on the timestamp t_1 , we divide it into three non-overlapping sub-streams $S_N^{t_0}$, $S_N^{t_1}$, and $S_N^{t_2}$, centered on timestamps t_0 , t_1 , and t_2 , respectively. The goal is to estimate the 6-DoF

Table 4: Statistics of the training and test set of synthetic dataset.

Dataset	Scene Indexes	Number of objectness	Number of graspness	Number of Spike Frames	Number of Scenes
Train	0–99	25,600	25,600	51,000	100
Seen	100–129	7,680	7,680	15,300	30
Similar	130–159	7,680	7,680	15,300	30
Novel	160–189	7,680	7,680	15,300	30

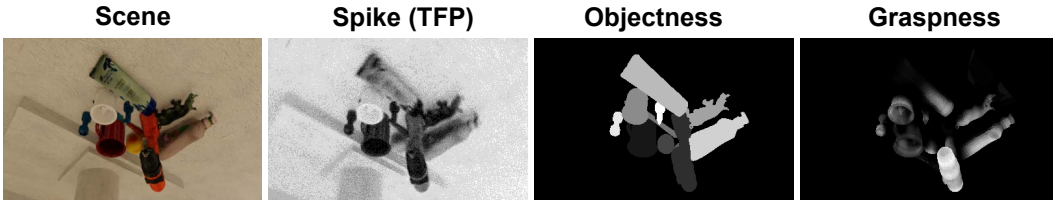


Figure 5: Visualize the results of examples in the synthetic dataset. From left to right are the scene map, TFP method reconstruction image of spike stream, objectiveness and graspness maps of the scene.

grasp pose corresponding to t_1 . Here, $S_N^{t_1}$ provides the essential spatial structure for estimating the grasp pose, while $S_N^{t_0}$ and $S_N^{t_2}$ provide temporal cues to improve consistency and robustness. Letting $S_n \in \{0, 1\}^{W \times H}$ denote the n -th spike frame, we predict the grasp pose at timestamp t_1 from the full spike stream $\{S_n\}, n = 0, \dots, k$, leveraging both spatial features and temporal continuity.

A.2.2 PROBLEM STATEMENT

A.3 DETAILS OF THE DATASET

A conventional active stereo depth system typically comprises an infrared projector, a pair of IR stereo cameras (left and right) and a color camera. We use the method from (Dai et al., 2022a; Zhang et al., 2024) that replicates this process, containing light pattern projection, capture, and segmentation. The simulator is implemented based on the Blender (Community, 2018) rendering engine.

A.3.1 SYNTHETIC DATASET

We construct a large-scale synthetic dataset using domain randomization and a spike simulator comprising two subsets. The training set contains 51,000 spike streams and 25,600 objectness/graspness maps from 100 scenes built with 88 distinct objects and randomized material properties (specular, transparent, diffuse). The test set contains 45,900 spike streams and 23,040 maps from 90 new scenes with the same 88 objects; it is partitioned into three splits: Seen, Similar and Novel, each with 30 scenes. Per scene, we provide 3–9 million grasp poses, generating more than 1.1 billion grasps in total sourced from GraspNet (Fang et al., 2020), as well as the binocular camera pose for each grasp scene. Detailed statistics are reported in Table 4. The samples of the synthetic dataset are shown in Fig. 5.

A.3.2 GRASPNESS GENERATION

A cluttered scene contains multiple objects and unrelated backgrounds. Therefore, it is important to generate the scene-level graspness in advance in the dataset. We computed the graspness map for each frame using segmentation and scene maps, as well as object-level grasp scores from the dataset, using the method similar to GSNet (Wang et al., 2021).

To address collisions, we reconstruct the scene using 3D object models and their 6-DoF poses. For each grasp $g_k^{i,j}$, we perform the collision check and assign a binary label $c_k^{i,j} \in \{0, 1\}$. We then

compute scene-level graspness by aggregating collision-free, high-quality grasps:

$$\begin{aligned}\tilde{s}_i^p &= \frac{\sum_{j=1}^V \sum_{k=1}^L \mathbf{1}(q_k^{i,j} > c) \cdot \mathbf{1}(c_k^{i,j})}{\sum_{j=1}^V |\mathcal{G}_{i,j}|}, i = 1, \dots, N, \\ \tilde{s}_i^v &= \left\{ \frac{\sum_{k=1}^L \mathbf{1}(q_k^{i,j} > c) \cdot \mathbf{1}(c_k^{i,j})}{|\mathcal{G}_{i,j}|} \mid 1 \leq j \leq V \right\}, i = 1, \dots, N.\end{aligned}\quad (10)$$

where $q_k^{i,j}$ is the grasp quality, τ is a quality threshold, V is the number of views, L the number of grasps per view, and $\mathcal{G}_{i,j}$ the candidate set at the scene point i and view j . Next, we project object points into the scene using their 6-DoF poses and, for each scene point, transfer graspness by nearest-neighbor association with the projected object points.

Finally, we normalize the scores per scene to obtain coherent maps.

$$\begin{aligned}\mathcal{S}^p &= \left\{ \frac{\tilde{s}_i^p - \min(\tilde{\mathcal{S}}^p)}{\max(\tilde{\mathcal{S}}^p) - \min(\tilde{\mathcal{S}}^p)} \mid i = 1, \dots, N \right\}, \\ \mathcal{S}^v &= \left\{ \frac{\tilde{s}_i^v - \mathbf{min}(\tilde{\mathcal{S}}^v)}{\mathbf{max}(\tilde{\mathcal{S}}^v) - \mathbf{min}(\tilde{\mathcal{S}}^v)} \mid i = 1, \dots, N \right\},\end{aligned}\quad (11)$$

where $\mathbf{min}(\cdot)$ denotes column-wise minimum:

$$\mathbf{min}(\tilde{\mathcal{S}}^v) = \left\{ \min_{i=1}^N \tilde{s}_{i(j)}^v \mid j = 1, \dots, V \right\}, \quad (12)$$

and so does $\mathbf{max}(\cdot)$. An example of the resulting scene-level graspness map is shown in Fig. 5.

A.3.3 EVALUATION METRICS

Before scoring, we apply SE(3) non-maximum suppression (NMS) to the predicted grasps and keep at most $N_{\text{per obj}}$ grasps per object. Let $\mathcal{G}_t = \{(\hat{G}_i, s_i)\}_{i=1}^{M_t}$ be the predictions for frame t , sorted by confidence s_i (descending) after NMS and per-object capping.

True-positive test (given friction μ). For each \hat{G}_i , define

$$y_i^{(\mu)} \in \{0, 1\} \quad (13)$$

to be 1 if \hat{G}_i (i) is assigned to a scene object, (ii) is collision-free, and (iii) satisfies force-closure under Coulomb friction coefficient μ ; otherwise 0.

Precision at the cutoff k .

$$\text{Prec}_t^{(\mu)}(k) = \frac{1}{k} \sum_{i=1}^k y_i^{(\mu)}, \quad k = 1, \dots, K_t, \quad (14)$$

where $K_t = \min(50, M_t)$. We chose the top 50 score of grasp poses predicted in this paper.

Frame-level average precision at μ .

$$\text{AP}_\mu(t) = \frac{1}{K_t} \sum_{k=1}^{K_t} \text{Prec}_t^{(\mu)}(k). \quad (15)$$

Dataset-level average precision (AP) at μ . For a test set of T frames,

$$\overline{\text{AP}}_\mu = \frac{1}{T} \sum_{t=1}^T \text{AP}_\mu(t). \quad (16)$$

AP_{0.8} and AP_{0.4}. These are $\overline{\text{AP}}_\mu$ evaluated at $\mu = 0.8$ and $\mu = 0.4$, respectively.

Overall AP (multi- μ average). Given a friction set M (e.g. $\{0.2, 0.4, 0.6, 0.8, 1.0, 1.2\}$),

$$\text{AP} = \frac{1}{|M|} \sum_{\mu \in M} \overline{\text{AP}}_\mu. \quad (17)$$

Specify the NMS thresholds in translation and rotation, the per-object cap $N_{\text{per obj}}$, the friction set M , and the results are averaged in the synthetic dataset. All of the above evaluation metrics are similar to COO (Lin et al., 2014) and (Wang et al., 2021).

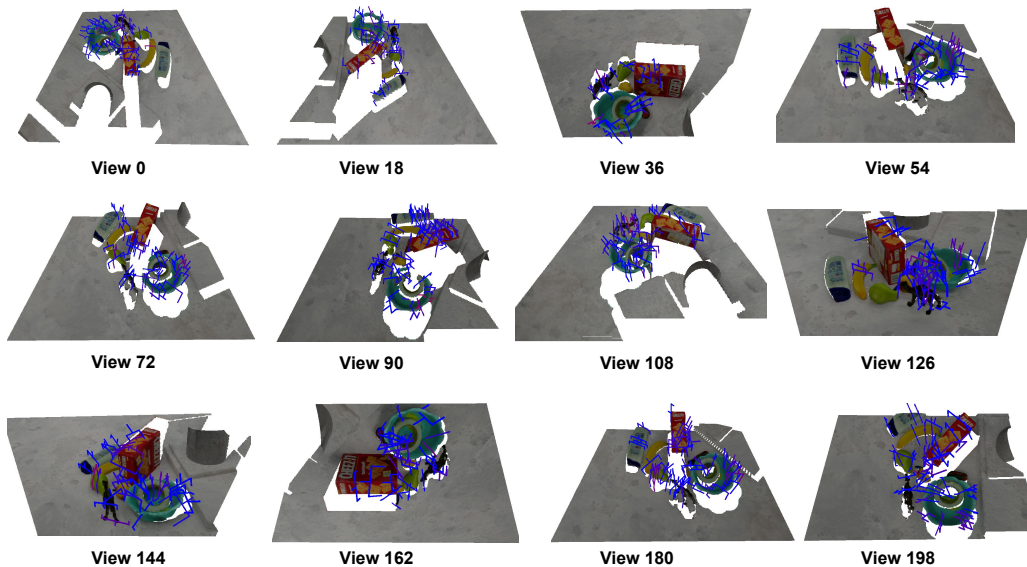


Figure 6: Visualization results of our method on the synthetic dataset in the single scene. We presented grasp poses predicted of 12 views in the scene.

A.4 MORE EXPERIMENTAL RESULTS

A.4.1 SCENE-LEVEL GRASP

We present a complete 6-DoF grasp pose sequence for a single scene within the synthetic dataset, capturing the full motion trajectory of objects throughout the dynamic environment. The complete scene is captured by the camera system rotating around the sphere, and the multi-view scene lays the foundation for subsequent dynamic grasping. We selected 12 of 256 views in a scene as illustrated in Fig. 6, the predicted 6-DoF grasp sequences effectively reconstruct the continuous evolution of the scene, accurately reflecting both spatial structure and temporal consistency. These results demonstrate the model’s ability to preserve coherent grasp across time, validating its effectiveness in handling visual inputs from different views. The supplementary materials in the zip file include continuously changing videos.

In addition, we conducted a qualitative comparison between SpikeGrasp and several state-of-the-art methods on the synthetic dataset. Our method consistently produces more accurate and visually coherent grasp poses in various scenes. Further qualitative results are provided to demonstrate the robustness and effectiveness of our approach.

A.4.2 COMPARISON EXPERIMENT

To visually illustrate the outstanding performance of our proposed SpikeGrasp algorithm in grasp pose detection, we performed a comparative visualization between SpikeGrasp, and two state-of-the-art algorithms, ASGrasp and GraspNet, as shown in Fig. 7. We randomly selected one scene from each test set for comparative analysis. The results show that SpikeGrasp predicts the top 50 grasp poses with higher overall confidence than the other algorithms. Compared to ASGrasp, SpikeGrasp predicts grasp poses that include a greater variety of objects. Relative to GraspNet, SpikeGrasp provides more intuitive and easily capture grasp poses. For instance, in scene 120, some of the top 50 grasp poses predicted by ASGrasp and GraspNet are not necessarily aimed at the objects but at the tabletop. In summary, through visual analysis, our SpikeGrasp algorithm predicts the top 50 grasp poses with greater reliability and precision for objects in cluttered scenes. It also covers a wider range of objects compared to other algorithms.

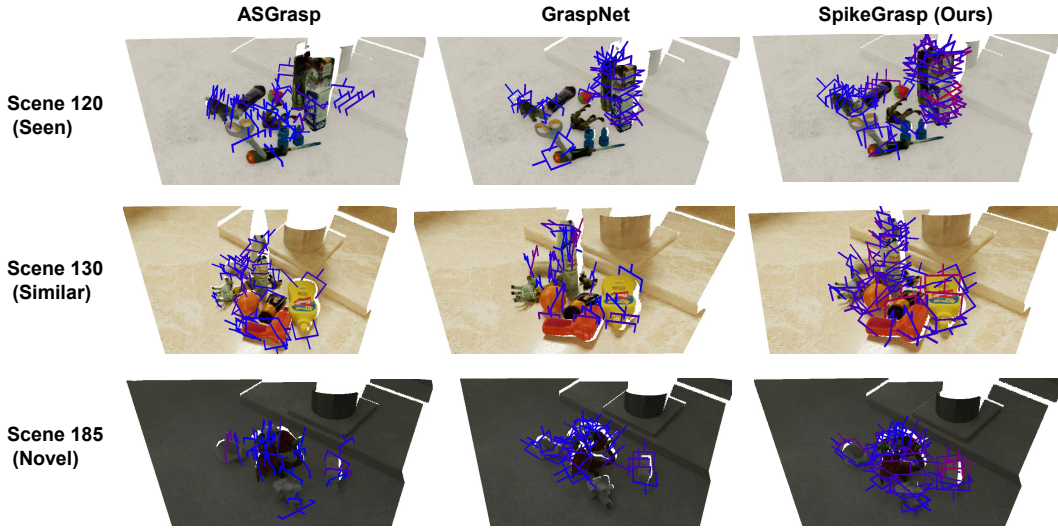


Figure 7: Visualizations of the top 50 grasp poses predicted by our SpikeGrasp algorithm compared to two state-of-the-art algorithms. A gripper-shaped geometry represents the grasp pose. Qualitative results covering Seen/Similar/Novel test.

A.4.3 SIMULATION EVALUATION

We evaluated grasping in NVIDIA Isaac Sim with a Franka Emika Panda and a Robotiq 2F-85 gripper. We construct 15 tabletop scenes, each populated with 6–8 objects instantiated from the CAD assets used to build our synthetic dataset. For each object, the policy predicts a 6-DoF end-effector pose in the spike camera signal sequences. We transform this pose to the world frame using known extrinsics, generate a pre-grasp by offsetting 10 cm along the approach axis, and execute a four-stage sequence: pre-grasp, approach, closure, and lift. Motion is performed via inverse kinematics with collision checks, and joint targets are tracked by Isaac’s articulation controller at 120 Hz. We allow up to three attempts per object.

A trial is successful if the object is lifted by 10 cm and held stably for one second without slip or secondary contact. We report the success rates as the fraction of objects successfully grasped across all scenes. Trained only on synthetic data, our model achieves 91.3% on Seen objects, 85.8% on Similar objects, and 70.9% on Novel objects. These results show a strong transfer from synthetic training to simulation and support the robustness of our approach.

A.5 BROADER IMPACTS

The proposed framework for 6-DoF grasp pose detection tasks from raw spike streams has strong potential to advance neuromorphic vision in various application scenarios. In the field of robotics, this method provides fine-grained perception support for precise manipulation, mapping, and motion planning, especially in highly dynamic or high-speed environments where traditional cameras typically perform poorly. Moreover, this framework is the first framework that can directly estimate 6-DoF grasp pose from raw stereo spike streams under supervised settings, enabling broader exploration of spike-based Visual tasks in both research and industrial applications.